HHS Public Access

Author manuscript

ACS Nano. Author manuscript; available in PMC 2017 March 23.

Published in final edited form as:

ACS Nano. 2013 December 23; 7(12): 10525–10533. doi:10.1021/nn4054683.

Physicochemical Properties of Nanoparticles Regulate Translocation across Pulmonary Surfactant Monolayer and Formation of Lipoprotein Corona

Guoqing Hu[†,*], **Bao Jiao**[†], **Xinghua Shi**[†], **Russell P. Valle**[‡], **Qihui Fan**[‡], and **Yi Y. Zuo**[‡,*]

[†]The State Key Laboratory of Nonlinear Mechanics (LNM), Institute of Mechanics, Chinese Academy of Sciences, Beijing, 100190, China

[‡]Department of Mechanical Engineering, University of Hawaii at Manoa, Honolulu, Hawaii 96822, United States

Abstract

Interaction with the pulmonary surfactant film, being the first line of host defense, represents the initial bio-nano interaction in the lungs. Such interaction determines the fate of the inhaled nanoparticles and their potential therapeutic or toxicological effect. Despite considerable progress in optimizing physicochemical properties of nanoparticles for improved delivery and targeting, the mechanisms by which inhaled nanoparticles interact with the pulmonary surfactant film are still largely unknown. Here, using combined *in vitro* and *in silico* methods, we show how hydrophobicity and surface charge of nanoparticles differentially regulate the translocation and interaction with the pulmonary surfactant film. While hydrophilic nanoparticles generally translocate quickly across the pulmonary surfactant film, a significant portion of hydrophobic nanoparticles are trapped by the surfactant film and encapsulated in lipid protrusions upon film compression. Our results support a novel model of pulmonary surfactant lipoprotein corona associated with inhaled nanoparticles of different physicochemical properties. Our data suggest that the study of pulmonary nanotoxicology and nanoparticle-based pulmonary drug delivery should consider this lipoprotein corona.

Graphical abstract

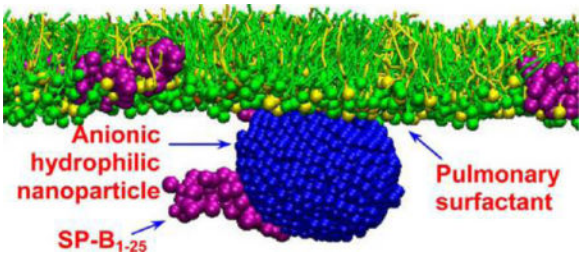

[*]Address correspondence to guoqing.hu@imech.ac.cn; yzuo@hawaii.edu.

Conflict of Interest: The authors declare no competing financial interest.

Supporting Information Available: Additional experimental data, detailed description of molecular dynamics simulation methods, supplemental simulation results, and video clips. This information is available free of charge *via* the Internet at http://pubs.acs.org.

Keywords

nanoparticle; protein corona; pulmonary surfactant; molecular dynamics

Nanoparticle-based pulmonary drug delivery has attracted significant attention due to its ease of administration, increased bioavailability, and reduced side-effects caused by high systemic dosage.[1,2] On the other hand, accumulating evidence suggests that engineered nanoparticles (NPs) may cause adverse health effects after inhalation, presumably similar to the toxicological effect of ultrafine particulate matters.[3,4] Due to their small size, a large portion of inhaled NPs can deposit in the distal regions of the lung, at which the aerosolized NPs must first interact with the pulmonary surfactant lining layer of alveoli.[5,6]

The pulmonary surfactant (PS) is a detergent-like substance synthesized by the type II alveolar epithelial cells. It is composed of approximately 90% lipids, mostly phospholipids, and 10% proteins by weight.[7] Four proteins have been found to be associated with PS, named SP-A, -B, -C, and -D. Among these proteins, SP-A and SP-D are large hydrophilic glycoproteins that are members of the Ca^{2+}-dependent carbohydrate-binding collectin family.[8] They are only weakly associated with the alveolar surfactant film but rather play a primary role in pulmonary host defense by binding to inhaled particles and pathogens to enhance phagocytic clearance.[8] SP-B and SP-C are smaller and hydrophobic proteins that play a crucial role in regulating the very low, near-zero surface tension in the lung.[9] SP-B and SP-C are known to be necessary for maintaining the normal biophysical function of PS and hence indispensable for air breathing.[9,10] Therefore, the PS plays a dual role of surface tension reduction and host defense in the lung. Increasing evidence suggests that interactions between PS and NPs are complicated. They are dependent on the physicochemical properties of the NPs[11,12] and also on the molecular composition,[13,14] dynamic surface phase behavior, and monolayer biomechanics of the PS.[15]

We first experimentally demonstrated the influence of NPs of different hydrophobicity on biophysical properties of an exogenous natural surfactant. Subsequently, we used molecular dynamics (MD) simulations to study the interaction mechanisms between PS monolayers and NPs of various physicochemical properties. MD simulations have provided invaluable insights into the translocation process of NPs through lipid membranes/bilayers.[16–18] Here, we have established a detailed MD model of the protein-containing PS monolayer that mimics the variation of lateral film pressure during the respiratory cycles. This model allowed us to probe lipid–protein interactions and to simulate NP translocation and interaction with the PS film. With combined experimental data and MD simulations, we concluded that a fine balance between electrostatic and hydrophobic interactions is responsible for the PS–NP interaction and the formation of a pulmonary surfactant lipoprotein corona.

RESULTS

Inhibition of Natural PS Exposed to Hydrophilic and Hydrophobic NPs

We first experimentally compared the effects of two representative NPs of different hydrophobicity on biophysical properties of an exogenous natural surfactant, *i.e.*, Infasurf. The two NPs studied here are made of hydroxyapatite (HA-NPs) and polystyrene (PST-NPs). The HA-NPs are derived from bone mineral and have been widely studied for biomedical applications due to their ideal biocompatibility and biodegradability.[19] The highly monodisperse PST-NPs are widely used as a model NP for studying nanotoxicology and bio-nano interactions.[20] These NPs share a similar hydrodynamic size (~90 nm) and are both negatively charged (−10 and −26 mV) at neutral pH, but are distinct in their surface hydrophobicity. While the HA-NPs are very hydrophilic, the PST-NPs are hydrophobic in nature.

As shown in Figure 1a, exposure to either NPs at 50 μg/mL (*i.e.*, 1% of surfactant phospholipids) inhibits the biophysical function of Infasurf, indicated by shifting the compression isotherm to the left; that is, more area reduction was needed to increase surface pressure. It should be noted that although the extent of isotherm shift with Infasurf by both NPs is similar, these two NPs generated different inhibition kinetics. As demonstrated in the Supplementary Figure S1, the hydrophobic PST-NPs induce faster inhibition than the hydrophilic HA-NPs. The compression isotherms ceased shifting after 7 h exposure to the HA-NPs,[15] but stabilized after only 1 h exposure to the PST-NPs. The more rapid inhibition of surface tension reduction by the hydrophobic PST-NPs relative to the hydrophilic HA-NPs clearly implies a difference in the NP–PS interaction mechanism.

Figure 1b shows the lateral structures of pure Infasurf film and Infasurf with 50 μg/mL (*i.e.*, 1% of surfactant phospholipids) HA-NPs or PST-NPs at characteristic surface pressures. Atomic force microscopy (AFM) topography images clearly reveal agglomerations of hydrophobic PST-NPs at the Infasurf monolayers. In contrast, no HA-NPs or particle agglomerations are detected at the interface, indicating that these hydrophilic NPs are not retained by the Infasurf monolayer at any surface pressure. Retention of the hydrophobic PST-NPs at the Infasurf monolayer is in line with their more potent inhibitory potential than the hydrophilic HA-NPs.

It is important to note that regardless of their different interaction behaviors, both NPs significantly altered the lateral structure of the Infasurf film. At surface pressures of 20–40 mN/m, both NPs inhibit phospholipid phase transition at the interfacial monolayer, as indicated by reduction in domain formation. This is consistent with the increased film compressibility shown by the compression isotherms.[7,21] At a surface pressure of 50 mN/m, both NPs alter the lateral film structure from a highly stable conformation of uniformly distributed lipid protrusions to an unstable nonuniform film structure with isolated and extended collapse patterns. Especially, the hydrophobic PST-NPs induce formation of extreme protrusions as high as 150 nm, which are observed on top of the 18 nm high multilayered lipid protrusions. As will be shown later by our *in silico* study, these extreme protrusions could correspond to hydrophobic PST-NPs encapsulated within lipid protrusions after local collapse of the PS film upon compression.

Our previous experimental study has demonstrated adsorption of surfactant proteins onto HA-NPs.[15] Since the surfactant proteins are expected to promote and stabilize fusion necks between bilayer protrusions and the interfacial monolayer,[22–24] alteration of lateral film structure and inhibition of surface activity after exposure to NPs can be indeed due to protein depletion or denaturation after adsorption onto NP surfaces, although the detailed molecular mechanism involved is still unclear.

Molecular Dynamics Simulations of NP Translocation across a Static PS Monolayer

To understand the mechanism of PS–NP interaction, we have established a detailed MD model to simulate particle translocation and interaction with the PS film. Our coarse-grained (CG) model system consists of 70 mol % dipalmitoyl phosphatidylcholine (DPPC) and 30 mol % palmitoyl-oleoyl phosphatidylglycerol (POPG), doped with 1.8 wt % SP-B peptide ($SP\text{-}B_{1–25}$) and 2.4 wt % SP-C. Although the chemical composition of this model system is considerably simpler than the natural PS, it contains both zwitterionic (PC) and anionic (PG) lipid headgroups, both disaturated (dipalmitoyl) and unsaturated (palmitoyl-oleoyl) acyl chains, and both hydrophobic surfactant protein peptides. Similar model systems have been experimentally proven to simulate certain biophysical properties of the natural PS, such as dynamic surface activity,[13] phospholipid phase separation, and squeeze-out of fluid phospholipids upon film compression.[25,26]

We first simulated the particle translocation through a static PS monolayer without lateral compression. As shown in Figure 2a, the equilibrium position of the NP after interacting with the PS monolayer is primarily determined by the hydrophobicity of the NP. While all hydrophilic NPs penetrate the monolayer, all hydrophobic NPs are trapped at the air–water interface (*i.e.*, $z = 0$). (See Supplementary Figure S2 for the coordinate system of our simulations and Figure S3 for schematics of MD models.) Compared to hydrophobicity, surface charge of the NP plays a secondary role in affecting the equilibrium position after interacting with the PS monolayer. For example, it appears that the cationic hydrophilic NP has an equilibrium position closer to the interfacial monolayer, in comparison with the neutral and anionic hydrophilic NPs. This is likely due to electrostatic attraction between anionic PG molecules at the interface and the cationic NP. (See Supplementary Figure S4 for additional MD simulations of lipid-NP interactions.)

To better understand the translocation process, we analyzed the potential of mean force (PMF) for the NP–PS interaction. As shown in Figure 2b, all hydrophilic NPs demonstrated local energy minima in the water phase; in contrast, the energy minima associated with all hydrophobic NPs are located at the air–water interface, indicating trapping of NPs by the surfactant monolayer. Figure 2c and d demonstrate the translocation process for two representative NPs, *i.e.*, an anionic hydrophilic NP and an anionic hydrophobic NP. They clearly demonstrate the effect of hydrophobicity of the NP on its translocation behavior, as predicted in Figure 2a and b. Interestingly, we found that the anionic hydrophilic NP adsorbs and pulls $SP\text{-}B_{1–25}$ (in purple) but not SP-C (in orange) out of the PS monolayer. This selective pulling behavior of the anionic NP has also been confirmed with interaction between the NP and dynamic PS monolayers, which will be discussed next.

Correlated Experimental and Molecular Simulation Study of Compressed PS Monolayer

To closely simulate the dynamic surface activity of PS, we subjected the surfactant monolayer to lateral compression that mimics exhalation. Meanwhile, we have compared our MD results to those experimentally obtained with Infasurf. As shown in Figure 3, compression isotherms obtained *in silico* and *in vitro* show good agreement. As the monolayer was compressed, surface pressure first increased rapidly and reached a plateau around the equilibrium spreading pressure of the PS (*i.e.*, 45–50 mN/m).[7] Although having different length and time scales, the MD simulations and AFM show qualitatively consistent molecular organization and lateral film structure during the compression process. Both MD and AFM clearly demonstrate that during the plateau region the PS film undergoes a monolayer-to-multilayer transition in which 3D multilayered lipid protrusions developed gradually from the 2D PS monolayer through localized film collapse. The MD simulations also show that the fusion necks/pores at which the monolayer collapsed are stabilized by SP-B/C (Supplementary Movie 1), consistent with previous MD.[23,24,27] This correlated MD and AFM observation confirms the nucleation-and-growth theory of overcompressed insoluble monolayers[28] and our previous experimental study on the collapse mechanism of PS monolayers.[29]

Molecular Dynamics Simulations of PS–NP Interactions

Having established the MD model for the dynamic natural PS, we studied the interaction between the PS monolayer and NPs of different hydrophobicities and surface charges. The CG models for NPs were built to be compatible with the MARTINI CG force field for proteins and lipids.[30,31] Each nanoparticle contained 1721 CG beads arranged in a face-centered-cubic arrangement. The diameter of the final NP was approximately 5 nm.

Figure 4 shows the interaction between hydrophilic NPs of different surface charges (a, cationic; b, neutral; and c, anionic) and the PS film, each at three different compression stages (monolayer, transition, and multilayer, corresponding to the three molecular areas shown in Figure 3). We found that all hydrophilic NPs quickly penetrate the surfactant monolayer. During the translocation process, the anionic NP (but not cationic or neutral NPs) selectively adsorbs and pulls SP-$B_{1–25}$ (but not SP-C) out of the interfacial monolayer (Supplementary Movies 2–4).

Figure 5 shows the PS interaction with hydrophobic NPs. It was found that upon contact with the PS monolayer, all hydrophobic NPs are immediately coated with a lipid monolayer and encapsulated within the lipid protrusions upon film compression (Supplementary Movies 5–7). To clearly demonstrate molecular interactions at the NP surfaces, we removed lipid molecules from the front view of the encapsulated NPs. As shown in the insets in the last row of Figure 5, all NPs are coated with a lipid monolayer *via* hydrophobic tail interactions. More interestingly, we found that, consistent with hydrophilic NPs in Figure 4, only the anionic NP (in blue) selectively adsorbs SP-$B_{1–25}$ (in purple). For cationic or neutral NPs, although a point contact is possible, SP-$B_{1–25}$ remains associated with the phospholipids without adsorbing onto the NP surfaces.

DISCUSSION

Hydrophobicity of NPs Determines Their Translocation across Natural PS Film

Both *in vitro* (Figure 1) and *in silico* (Figures 2, 4, and 5) studies suggest that surface hydrophobicity of NPs determines their translocation across the PS film. While the hydrophilic NPs quickly penetrate the PS monolayer, a portion of the hydrophobic NPs are trapped by the PS monolayer. Surface charge of the NPs plays only a secondary role in affecting the NP translocation across the PS monolayer. However, it should be noted that the alveolocapillary translocation pathway for inhaled NPs consists of the alveolar epithelium cells, extracellular basement membrane, and capillary endothelium cells. The PS film at the air–water interface of alveoli is only the initial barrier of this pathway. The actual translocation behavior of engineered NPs can be complicated and depends on both the physicochemical properties of NPs and the model used for evaluation.[32] Nevertheless, our *in vitro* and *in silico* findings on the retention of hydrophobic NPs are in good agreement with previous *ex vivo* and *in vivo* translocation data.[33–35] Nemmar *et al.* found that after intratracheal instillation in isolated perfused rabbit lungs PST-NPs (24–190 nm) with different charges were mainly located in the alveolar region without translocation into the vascular compartment.[33] Chen *et al.* found that only 1–2% intratracheally instilled radiolabeled PST-NPs (56–200 nm) in rats can translocate from the lungs.[34] Similarly, Mills *et al.* found that carbon-based NPs, even at very small sizes (4–20 nm), remained in the lungs up to 6 h after inhalation by healthy volunteers.[35]

Surface Charge of NPs Regulates Formation of PS Lipoprotein Corona

Adsorption of surfactant proteins and/or lipids onto surfaces of engineered nanomaterials, such as multiwalled[36] and single-walled carbon nanotubes[37] and metal oxide NPs,[38,39] has been reported. However, these previous studies mainly focused on the two large hydrophilic glycoproteins SP-A and SP-D. Different from previous studies, the present MD simulations focused on the two small apolipoproteins SP-B and SP-C. Both proteins are hydrophobic, positively charged (pI = 8–9), tightly associated with the alveolar surfactant lining layer, and essential for regulating surface activity of PS film during normal tidal breathing.[9,10] We found that the anionic NP selectively adsorbs SP-$B_{1–25}$, but not SP-C. (See Supplemental Figure S5 for additional MD simulations that confirmed the specificity of this interaction.) Consequently, the anionic hydrophilic NP can pull SP-$B_{1–25}$, but not SP-C, out of the interfacial surfactant monolayer (Figure 4). Although the anionic hydrophobic NP is trapped by the PS film, it also selectively adsorbs SP-$B_{1–25}$ onto the particle surface (Figure 5).

Both experimental and MD studies have shown that SP-$B_{1–25}$ represents certain properties of the full-length SP-B.[40,41] As shown in the Supplemental Figure S6, SP-$B_{1–25}$ contains the 1–25 N-terminal residues of the SP-B molecule. Compared to the 35 amino acid long SP-C molecule, SP-$B_{1–25}$ has a higher positive charge density but is significantly less hydrophobic than SP-C. Therefore, compared to SP-C, SP-$B_{1–25}$ is subject to a higher electrostatic pulling by the anionic NP but less hydrophobic retention due to the interfacial phospholipid monolayer, thus being susceptible to being pulled out of the interfacial monolayer. Our data therefore indicate that a fine balance between electrostatic and hydrophobic interactions is responsible for the NP translocation and interaction with the PS monolayer.

Adsorption of surfactant protein peptides onto anionic NPs can have a significant adverse impact on the biophysical function of the PS. Protein denaturation and conformational change are not unexpected after adsorbing onto the NP surfaces. This PS–NP interaction mechanism may explain the inhibitory effect of NPs on Infasurf (Figure 1). This interaction mechanism is also in line with recent experimental data reported by Beck-Broichsitter *et al.*[12] These workers found that negatively charged polymeric NPs significantly inhibited surface activity of a protein-containing natural PS, while positively charged NPs showed no effect on surface activity. They also found that hydrophobic NPs inhibited the natural PS more than hydrophilic NPs, likely due to retention of the NPs at the surfactant film.[12] It has been reported that reducing SP-B content to less than 25% of normal levels in adult mice caused lethal respiratory failure.[42] The SP-B half-life in neonates was found to be about 10 h, which turns over much quicker than phospholipids.[43] Hence, the rapid surfactant inhibition induced by NPs, *i.e.*, effective within 1 h after particle exposure, can be indeed physiologically relevant.

Lesniak *et al.* have shown that during endocytosis NPs can acquire a corona from native biomolecules of the cell membrane, thus inducing cytotoxicity.[44] The biomolecular corona formed when passing through endogenous biological media determines the biological identity of the NPs and hence their subsequent recognition by the biological machinery.[6] Together with previous studies on surfactant glycoproteins (SP-A and SP-D)[38,39] and phospholipids,[37] our MD simulations suggest that inhaled NPs can acquire a lipoprotein corona from endogenous PS and may consequently inhibit the biophysical function of the PS. The structure of this PS lipoprotein corona depends on the physicochemical properties of the inhaled NPs, perhaps similar to the high-density lipoprotein corona mediated by apolipoprotein A-I.[45]

Implications to Nanotoxicology and Pulmonary Drug Delivery

Our findings have implications for understanding nanotoxicology and design of NP-based pulmonary drug delivery. Since the PS film forms the first alveolar capillary barrier against inhaled particles, any *in vitro* study of inhalation nanotoxicology or pulmonary drug delivery should consider the NP–PS lipoprotein complex instead of the pristine NPs. It has been shown that incubating NPs with protein-containing natural PS can significantly reduce subsequent adsorption of cell plasma proteins onto the NP surfaces,[46] trigger NP phagocytosis,[39,47] affect the oxidative potential of multiwalled carbon nanotubes,[48,49] and even vary the biodistribution and biokinetics of NPs translocated into secondary organs.[50,51] All these results are consistent with the formation of the PS lipoprotein corona. These results suggest that the PS lipoprotein corona not only affects the biophysical properties of the PS film but also plays an important role in regulating subsequent biomolecular exchange on NP surfaces, interaction with lung cells, and particle translocation to various organs and tissues.

For NPs made for pulmonary drug delivery, our simulations suggest that hydrophobic NPs, such as carbon-based nanomaterials, can be trapped at the surfactant lining layer and consequently lead to prolonged retention and increased inflammation potentials.[52,53] Hydrophilic NPs are ideal for systemic drug delivery due to their rapid translocation to secondary organs and tissues.[50] However, anionic NPs (such as the carboxylic-modified

NPs) may inhibit the biophysical function of the endogenous surfactant by binding to surfactant protein(s). Since cationic NPs (such as the amino-modified NPs) may be taken up by cells and cause acute cytotoxicity,[50] our data suggest that neutral NPs might be the safest for pulmonary drug delivery.

CONCLUSIONS

With combined MD simulation and experimental observation, our data suggest formation of a PS lipoprotein corona on inhaled NPs. Hydrophobicity and surface charges of the NPs were found to play an important role in regulating particle translocation across the PS film and formation of the lipoprotein corona. Other physicochemical properties, such as size, shape/aspect ratio, and aggregation state of the NPs, may also affect their interaction potential with PS, thus being subjects of our future study. Together with previous experimental studies, our simulations indicate that interaction with the PS and formation of lipoprotein corona not only affect the biophysical properties of the PS film but also play an important role in regulating subsequent biomolecular exchange on NP surfaces, interaction with lung cells, and particle translocation to various organs and tissues. Our data therefore suggest that any *in vitro* study of inhalation nanotoxicology or NP-based pulmonary drug delivery should consider this NP–PS lipoprotein complex instead of the pristine NPs.

METHODS

Pulmonary Surfactant

Infasurf (calfactant) is a gift from ONY, Inc. (Amherst, NY, USA). It is a modified natural surfactant prepared from lung lavage of newborn calves by centrifugation and organic solvent extraction. Infasurf contains all hydrophobic components of the bovine natural surfactant.[25] Hydrophilic surfactant protein (SP-A), however, was removed during the extraction process. Infasurf was stored frozen in sterilized vials with an initial concentration of 35 mg total phospholipids per milliliter. On the day of experiment it was diluted to 5 mg/mL by a saline buffer of 0.9% NaCl, 1.5 mM $CaCl_2$, and 2.5 mM HEPES, adjusted to pH 7.0.

Nanoparticles

Hydroxyapatite nanoparticles (HA-NPs) were synthesized by a technique described elsewhere.[15,54] Polystyrene nanoparticles (PST-NPs) with a standard size of 92 ± 3 nm were purchased from Thermo Scientific (3090A Nanosphere Size Standards, Fremont, CA, USA). These PST-NPs are NIST traceable particle size standards used for calibrating electron and atomic force microscopes. Both NPs were characterized for their hydrodynamic size, surface charge, and surface hydrophobicity. The hydrodynamic size and zeta potential of the NPs were determined at a dilute particle concentration of 0.01 mg/mL under the same buffering condition of the natural PS, *i.e.*, 0.9% NaCl, 1.5 mM $CaCl_2$, and 2.5 mM HEPES, at pH 7.0. The hydrodynamic sizes of HA-NPs and PST-NPs were measured to be ~93 and ~92 nm using a Brookhaven 90Plus/BI-MAS particle sizer (Holtsville, NY, USA). Zeta potentials of the HA-NPs and PST-NPs were determined to be about −10 and −26 mV, using a

Brookhaven Zetaplus zeta potential analyzer. Hydrophobicity of the NPs was confirmed by studying adsorption at the air–water interface, measured by surface tension variations.[15]

Langmuir–Blodgett Trough

Spread, compression, and Langmuir–Blodgett (LB) transfer of surfactant films were conducted with a LB trough (KSV Nima, Coventry, UK) at room temperature (20 ± 1 °C). A detailed experimental protocol can be found elsewhere.[15] Briefly, HA-NPs or PST-NPs were first mixed and co-spread with 5 mg/mL Infasurf at a ratio of 1% by weight. The co-spread films were compressed at a rate of 20 cm^2/min, namely, 0.1% initial surface area per second. For AFM imaging, Infasurf films at the air–water interface were transferred to the surface of freshly cleaved mica using the LB technique. Surfactant films at controlled constant surface pressure were deposited onto the mica surface by elevating the previously submerged mica vertically through the air–water interface at a rate of 1 mm/min. Deposited films were scanned by AFM within 2 h of deposition.

AFM

Topographical images were obtained using an Innova AFM (Bruker, Santa Barbara, CA, USA). Samples were scanned in air. Each sample was characterized at multiple locations with various scan areas to ensure the detection of representative structures. Both contact mode and tapping mode were used. The different scan modes gave equivalent results. A silicon nitride cantilever with a spring constant of 0.12 N/m and a nominal tip radius of 2 nm was used in contact mode, and a silicon probe with a resonance frequency of 300 kHz and a spring constant of 40 N/m was used in tapping mode. Analysis of the AFM images was performed using Nanoscope software (ver. 7.30).

Molecular Dynamics Simulations

The entire system was simulated with coarse-grained models, which allow molecular simulations at a larger length-scale and longer time-scale than all-atom models. A detailed description about our simulations can be found in the Supporting Information. Briefly, each PS monolayer contained 1120 CG DPPC (green) and 480 CG POPG (yellow) molecules (7:3), doped with 7 CG SP-$B_{1–25}$ (purple) and 7 CG SP-C (orange) molecules. The CG models for NPs were built to be compatible with the MARTINI CG force field for proteins and lipids.[30,31] Each nanoparticle contained 1721 CG beads arranged in a face-centered-cubic arrangement. The diameter of the final NP was approximately 5 nm. The CG bead types P2 and C1 were used for constructing the neutral (black) hydrophilic and hydrophobic NPs, respectively. Qda and Qa were used to modify the surface charge of the particle. Cationic particles are shown in red, and anionic particles are shown in blue. The water slab contained 158 418 CG water beads and 862 Na^+ ions to neutralize the system. Please refer to Supplementary Figure S3 for the schematics and color schemes of the simulated CG molecules and particles. All simulations were performed using GROMACS 4.5.4.[55]

Supplementary Material

Refer to Web version on PubMed Central for supplementary material.

Acknowledgments

The authors thank Fred Possmayer for insightful comments on our manuscript. We thank Walter Klein at ONY Inc. for donation of Infasurf samples, and Joachim Loo for synthesizing the hydroxyapatite nanoparticles. The MD simulations were performed on TianHe-1(A) at the National Supercomputing Center in Tianjin. This work was supported by MOST 2011CB707604, NSFC 11272321 (G.H.), NSFC 11272327 (X.S.), and NSF Grant No. CBET-1236596 (Y.Y.Z.).

REFERENCES AND NOTES

1. Patton JS, Byron PR. Inhaling Medicines: Delivering Drugs to the Body through the Lungs. Nat Rev Drug Discovery. 2007; 6:67–74. [PubMed: 17195033]
2. Bailey MM, Berkland CJ. Nanoparticle Formulations in Pulmonary Drug Delivery. Med Res Rev. 2009; 29:196–212. [PubMed: 18958847]
3. Oberdorster G, Oberdorster E, Oberdorster J. Nanotoxicology: An Emerging Discipline Evolving from Studies of Ultrafine Particles. Environ Health Perspect. 2005; 113:823–839. [PubMed: 16002369]
4. Nel A, Xia T, Madler L, Li N. Toxic Potential of Materials at the Nanolevel. Science. 2006; 311:622–627. [PubMed: 16456071]
5. Nel AE, Madler L, Velegol D, Xia T, Hoek EM, Somasundaran P, Klaessig F, Castranova V, Thompson M. Understanding Biophysicochemical Interactions at the Nano-Bio Interface. Nat Mater. 2009; 8:543–557. [PubMed: 19525947]
6. Monopoli MP, Aberg C, Salvati A, Dawson KA. Biomolecular Coronas Provide the Biological Identity of Nanosized Materials. Nat Nanotechnol. 2012; 7:779–786. [PubMed: 23212421]
7. Zuo YY, Veldhuizen RA, Neumann AW, Petersen NO, Possmayer F. Current Perspectives in Pulmonary Surfactant-Inhibition, Enhancement and Evaluation. Biochim Biophys Acta. 2008; 1778:1947–1977. [PubMed: 18433715]
8. McCormack FX, Whitsett JA. The Pulmonary Collectins, SP-A and SP-D, Orchestrate Innate Immunity in the Lung. J Clin Invest. 2002; 109:707–712. [PubMed: 11901176]
9. Perez-Gil J. Structure of Pulmonary Surfactant Membranes and Films: The Role of Proteins and Lipid-Protein Interactions. Biochim Biophys Acta. 2008; 1778:1676–1695. [PubMed: 18515069]
10. Whitsett JA, Weaver TE. Hydrophobic Surfactant Proteins in Lung Function and Disease. N Engl J Med. 2002; 347:2141–2148. [PubMed: 12501227]
11. Schleh C, Muhlfeld C, Pulskamp K, Schmiedl A, Nassimi M, Lauenstein HD, Braun A, Krug N, Erpenbeck VJ, Hohlfeld JM. The Effect of Titanium Dioxide Nanoparticles on Pulmonary Surfactant Function and Ultrastructure. Respir Res. 2009; 10:90. [PubMed: 19793393]
12. Beck-Broichsitter M, Ruppert C, Schmehl T, Guenther A, Betz T, Bakowsky U, Seeger W, Kissel T, Gessler T. Biophysical Investigation of Pulmonary Surfactant Surface Properties upon Contact with Polymeric Nanoparticles. In Vitro Nanomed. 2011; 7:341–350.
13. Bakshi MS, Zhao L, Smith R, Possmayer F, Petersen NO. Metal Nanoparticle Pollutants Interfere with Pulmonary Surfactant Function *in Vitro*. Biophys J. 2008; 94:855–868. [PubMed: 17890383]
14. Sachan AK, Harishchandra RK, Bantz C, Maskos M, Reichelt R, Galla HJ. High-Resolution Investigation of Nanoparticle Interaction with a Model Pulmonary Surfactant Monolayer. ACS Nano. 2012; 6:1677–1687. [PubMed: 22288983]
15. Fan Q, Wang YE, Zhao X, Loo JS, Zuo YY. Adverse Biophysical Effects of Hydroxyapatite Nanoparticles on Natural Pulmonary Surfactant. ACS Nano. 2011; 5:6410–6416. [PubMed: 21761867]
16. Qiao R, Roberts AP, Mount AS, Klaine SJ, Ke PC. Translocation of C60 and its Derivatives across a Lipid Bilayer. Nano Lett. 2007; 7:614–619. [PubMed: 17316055]
17. Wong-Ekkabut J, Baoukina S, Triampo W, Tang IM, Tieleman DP, Monticelli L. Computer Simulation Study of Fullerene Translocation through Lipid Membranes. Nat Nanotechnol. 2008; 3:363–368. [PubMed: 18654548]

18. Shi X, von dem Bussche A, Hurt RH, Kane AB, Gao H. Cell Entry of One-Dimensional Nanomaterials Occurs by Tip Recognition and Rotation. Nat Nanotechnol. 2011; 6:714–719. [PubMed: 21926979]
19. Loo SC, Moore T, Banik B, Alexis F. Biomedical Applications of Hydroxyapatite Nanoparticles. Curr Pharm Biotechnol. 2010; 11:333–342. [PubMed: 20199383]
20. Lundqvist M, Stigler J, Elia G, Lynch I, Cedervall T, Dawson KA. Nanoparticle Size and Surface Properties Determine the Protein Corona with Possible Implications for Biological Impacts. Proc Natl Acad Sci US A. 2008; 105:14265–14270.
21. Casals C, Canadas O. Role of Lipid Ordered/Disordered Phase Coexistence in Pulmonary Surfactant Function. Biochim Biophys Acta. 2012; 1818:2550–2562. [PubMed: 22659676]
22. Chavarha M, Loney RW, Kumar K, Rananavare SB, Hall SB. Differential Effects of the Hydrophobic Surfactant Proteins on the Formation of Inverse Bicontinuous Cubic Phases. Langmuir. 2012; 28:16596–16604. [PubMed: 23140329]
23. Baoukina S, Tieleman DP. Lung Surfactant Protein SP-B Promotes Formation of Bilayer Reservoirs from Monolayer and Lipid Transfer between the Interface and Subphase. Biophys J. 2011; 100:1678–1687. [PubMed: 21463581]
24. Baoukina S, Tieleman DP. Direct Simulation of Protein-Mediated Vesicle Fusion: Lung Surfactant Protein B. Biophys J. 2010; 99:2134–2142. [PubMed: 20923647]
25. Zhang H, Fan Q, Wang YE, Neal CR, Zuo YY. Comparative Study of Clinical Pulmonary Surfactants Using Atomic Force Microscopy. Biochim Biophys Acta. 2011; 1808:1832–1842. [PubMed: 21439262]
26. Keating E, Zuo YY, Tadayyon SM, Petersen NO, Possmayer F, Veldhuizen RA. A Modified Squeeze-Out Mechanism for Generating High Surface Pressures with Pulmonary Surfactant. Biochim Biophys Acta. 2012; 1818:1225–1234. [PubMed: 22206628]
27. Baoukina S, Monticelli L, Risselada HJ, Marrink SJ, Tieleman DP. The Molecular Mechanism of Lipid Monolayer Collapse. Proc Natl Acad Sci USA. 2008; 105:10803–10808. [PubMed: 18669655]
28. Vollhardt D, Retter U. Nucleation in Insoluble Monolayers 0.1. Nucleation and Growth-Model for Relaxation of Metastable Monolayers. J Phys Chem. 1991; 95:3723–3727.
29. Zhang H, Wang YE, Fan Q, Zuo YY. On the Low Surface Tension of Lung Surfactant. Langmuir. 2011; 27:8351–8358. [PubMed: 21650180]
30. Marrink SJ, de Vries AH, Mark AE. Coarse Grained Model for Semiquantitative Lipid Simulations. J Phys Chem B. 2004; 108:750–760.
31. Monticelli L, Kandasamy SK, Periole X, Larson RG, Tieleman DP, Marrink SJ. The MARTINI Coarse-Grained Force Field: Extension to Proteins. J Chem Theory Comput. 2008; 4:819–834. [PubMed: 26621095]
32. Kendall M, Holgate S. Health Impact and Toxicological Effects of Nanomaterials in the Lung. Respirology. 2012; 17:743–758. [PubMed: 22449246]
33. Nemmar A, Hamoir J, Nemery B, Gustin P. Evaluation of Particle Translocation across the Alveolo-Capillary Barrier in Isolated Perfused Rabbit Lung Model. Toxicology. 2005; 208:105–113. [PubMed: 15664437]
34. Chen J, Tan M, Nemmar A, Song W, Dong M, Zhang G, Li Y. Quantification of Extrapulmonary Translocation of Intratracheal-Instilled Particles *in Vivo* in Rats: Effect of Lipopolysaccharide. Toxicology. 2006; 222:195–201. [PubMed: 16584826]
35. Mills NL, Amin N, Robinson SD, Anand A, Davies J, Patel D, de la Fuente JM, Cassee FR, Boon NA, Macnee W, et al. Do Inhaled Carbon Nanoparticles Translocate Directly into the Circulation in Humans? Am J Respir Crit Care Med. 2006; 173:426–431. [PubMed: 16339922]
36. Salvador-Morales C, Townsend P, Flahaut E, Venien-Bryan C, Vlandas A, Green MLH, Sim RB. Binding of Pulmonary Surfactant Proteins to Carbon Nanotubes; Potential for Damage to Lung Immune Defense Mechanisms. Carbon. 2007; 45:607–617.
37. Kapralov AA, Feng WH, Amoscato AA, Yanamala N, Balasubramanian K, Winnica DE, Kisin ER, Kotchey GP, Gou P, Sparvero LJ, et al. Adsorption of Surfactant Lipids by Single-Walled Carbon Nanotubes in Mouse Lung upon Pharyngeal Aspiration. ACS Nano. 2012; 6:4147–4156. [PubMed: 22463369]

38. Schulze C, Schaefer UF, Ruge CA, Wohlleben W, Lehr CM. Interaction of Metal Oxide Nanoparticles with Lung Surfactant Protein A. Eur J Pharm Biopharm. 2011; 77:376–383. [PubMed: 21056657]
39. Ruge CA, Schaefer UF, Herrmann J, Kirch J, Canadas O, Echaide M, Perez-Gil J, Casals C, Muller R, Lehr CM. The Interplay of Lung Surfactant Proteins and Lipids Assimilates the Macrophage Clearance of Nanoparticles. PLoS One. 2012; 7:e40775. [PubMed: 22802970]
40. Longo ML, Bisagno AM, Zasadzinski JA, Bruni R, Waring AJ. A Function of Lung Surfactant Protein SP-B. Science. 1993; 261:453–456. [PubMed: 8332910]
41. Choe S, Chang R, Jeon J, Violi A. Molecular Dynamics Simulation Study of a Pulmonary Surfactant Film Interacting with a Carbonaceous Nanoparticle. Biophys J. 2008; 95:4102–4114. [PubMed: 18923102]
42. Melton KR, Nesslein LL, Ikegami M, Tichelaar JW, Clark JC, Whitsett JA, Weaver TE. SP-B Deficiency Causes Respiratory Failure in Adult Mice. Am J Physiol. 2003; 285:L543–L549.
43. Simonato M, Baritussio A, Vedovelli L, Lamonica G, Carnielli VP, Cogo PE. Surfactant Protein B Amount and Kinetics in Newborn Infants: An Optimized Procedure. J Mass Spectrom. 2012; 47:1415–1419. [PubMed: 23147816]
44. Lesniak A, Fenaroli F, Monopoli MP, Aberg C, Dawson KA, Salvati A. Effects of the Presence or Absence of a Protein Corona on Silica Nanoparticle Uptake and Impact on Cells. ACS Nano. 2012; 6:5845–5857. [PubMed: 22721453]
45. Hellstrand E, Lynch I, Andersson A, Drakenberg T, Dahlback B, Dawson KA, Linse S, Cedervall T. Complete High-Density Lipoproteins in Nanoparticle Corona. FEBS J. 2009; 276:3372–3381. [PubMed: 19438706]
46. Sund J, Alenius H, Vippola M, Savolainen K, Puustinen A. Proteomic Characterization of Engineered Nanomaterial-Protein Interactions in Relation to Surface Reactivity. ACS Nano. 2011; 5:4300–4309. [PubMed: 21528863]
47. Ruge CA, Kirch J, Canadas O, Schneider M, Perez-Gil J, Schaefer UF, Casals C, Lehr CM. Uptake of Nanoparticles by Alveolar Macrophages Is Triggered by Surfactant Protein A. Nanomedicine. 2011; 7:690–693. [PubMed: 21839052]
48. Gasser M, Wick P, Clift MJ, Blank F, Diener L, Yan B, Gehr P, Krug HF, Rothen-Rutishauser B. Pulmonary Surfactant Coating of Multi-Walled Carbon Nanotubes (MWCNTs) Influences their Oxidative and Pro-inflammatory Potential *in Vitro*. Part Fibre Toxicol. 2012; 9:17. [PubMed: 22624622]
49. Schleh C, Kreyling WG, Lehr CM. Pulmonary Surfactant is Indispensable in Order to Simulate the *in Vivo* Situation. Part Fibre Toxicol. 2013; 10:6. [PubMed: 23531298]
50. Choi HS, Ashitate Y, Lee JH, Kim SH, Matsui A, Insin N, Bawendi MG, Semmler-Behnke M, Frangioni JV, Tsuda A. Rapid Translocation of Nanoparticles from the Lung Airspaces to the Body. Nat Biotechnol. 2010; 28:1300–1303. [PubMed: 21057497]
51. Kreyling WG, Hirn S, Schleh C. Nanoparticles in the Lung. Nat Biotechnol. 2010; 28:1275–1276. [PubMed: 21139613]
52. Poland CA, Duffin R, Kinloch I, Maynard A, Wallace WA, Seaton A, Stone V, Brown S, Macnee W, Donaldson K. Carbon Nanotubes Introduced into the Abdominal Cavity of Mice Show Asbestos-Like Pathogenicity in a Pilot Study. Nat Nanotechnol. 2008; 3:423–428. [PubMed: 18654567]
53. Ryman-Rasmussen JP, Cesta MF, Brody AR, Shipley-Phillips JK, Everitt JI, Tewksbury EW, Moss OR, Wong BA, Dodd DE, Andersen ME, et al. Inhaled Carbon Nanotubes Reach the Subpleural Tissue in Mice. Nat Nanotechnol. 2009; 4:747–751. [PubMed: 19893520]
54. Ng S, Guo J, Ma J, Loo SC. Synthesis of High Surface Area Mesostructured Calcium Phosphate Particles. Acta Biomater. 2010; 6:3772–3781. [PubMed: 20233611]
55. Lindahl E, Hess B, van der Spoel D. GROMACS 3.0: A Package for Molecular Simulation and Trajectory Analysis. J Mol Model. 2001; 7:306–317.

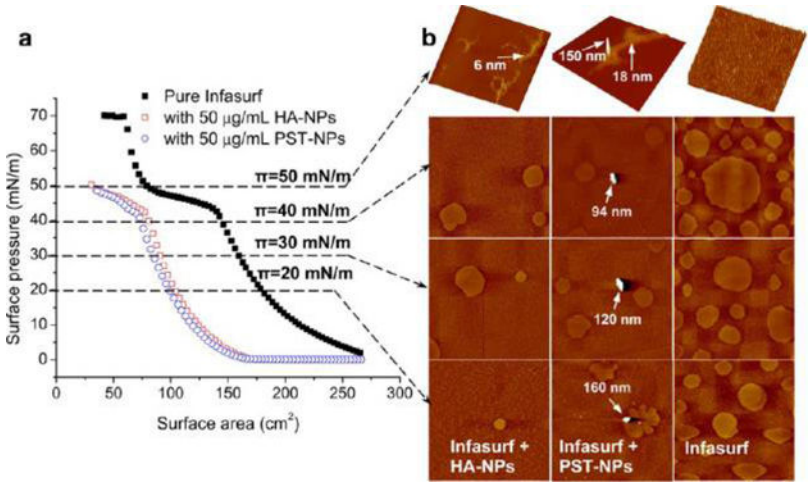

Figure 1.

Experimental interactions between a natural pulmonary surfactant film (Infasurf) and representative hydrophilic NPs (i.e., hydroxyapatite, HA-NPs) or hydrophobic NPs (i.e., polystyrene, PST-NPs). (a) Effect of 50 μg/mL HA-NPs or PST-NPs (i.e., 1% of surfactant phospholipids) on the compression isotherm of Infasurf at equilibrium (i.e., no more time-dependent isotherm shifting). (b) Lateral structures of the films with and without exposure to NPs, shown at four characteristic surface pressures (π) of 20, 30, 40, and 50 mN/m. The scan area of the AFM images is 20 × 20 μm; the full z-range is 5 nm for monolayers (at 20, 30, and 40 mN/m), 20 nm for multilayers exposed to HA-NPs (at 50 mN/m), and 150 nm for multilayers exposed to PST-NPs (at 50 mN/m). It is found that both HA-NPs and PST-NPs inhibit the biophysical function of Infasurf, as indicated by shifting the compression isotherm to the left; that is, more area reduction is required to increase surface pressure. AFM reveals that both HA-NPs and PST-NPs inhibit the phospholipid phase transition (at low π) and monolayer-to-multilayer transformation (at high π) of Infasurf. Variations of lateral film structure at 50 mN/m from a uniform matrix structure to a nonuniform structure of isolated high collapse patterns result in unstable surfactant films and thus lead to surfactant inhibition. More importantly, AFM reveals different interaction behaviors between these two NPs of different hydrophobicity and the Infasurf film. While the hydrophilic HA-NPs are not retained by the Infasurf film, a portion of the hydrophobic PST-NPs and agglomerations (labeled by arrows) are trapped by the surfactant films.

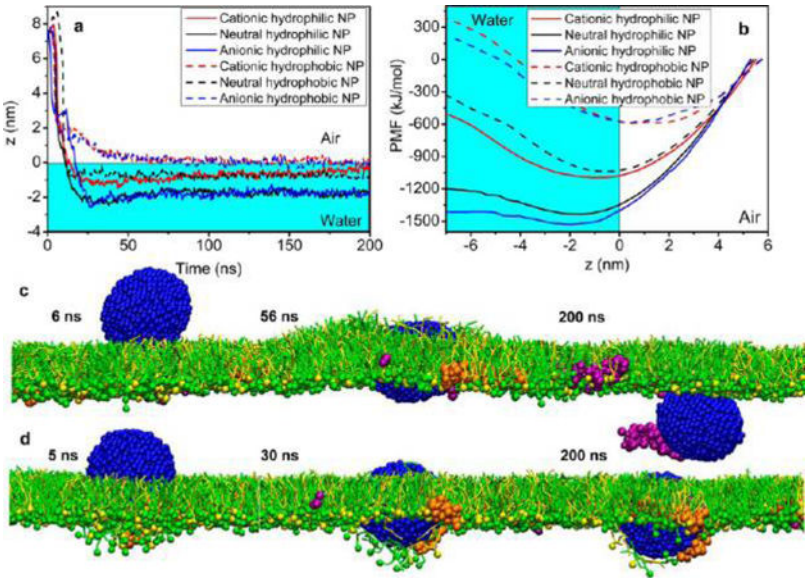

Figure 2.

Simulated translocation of a nanoparticle (NP) of different surface charges (cationic, neutral, and anionic) and hydrophobicities (hydrophilic and hydrophobic) through a pulmonary surfactant monolayer. (a) Equilibrium position (z) of the NP. (b) Potential of mean force (PMF) for the interaction between the NP and the pulmonary surfactant monolayer. (c, d) Simulated translocation process for two representative NPs, i.e., an anionic hydrophilic NP (c) and an anionic hydrophobic NP (d), with the increasing simulation time (in ns). Note that the anionic hydrophilic NP adsorbs and pulls SP-B1–25 (in purple) out of the surfactant monolayer. Color code used in MD simulations: DPPC in green; POPG in yellow; SP-B1–25 in purple; SP-C in orange; and anionic particle in blue.

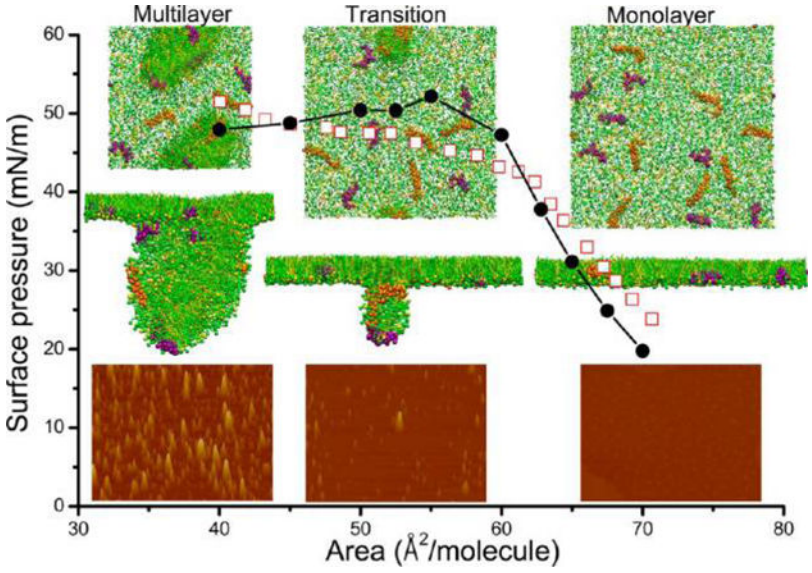

Figure 3.

Comparison of computer simulated and experimentally obtained molecular organization and lateral structure of a pulmonary surfactant monolayer upon compression. The solid circles indicate the computer-simulated compression isotherm, while the open squares indicate the experimentally measured compression isotherm using a Langmuir balance. The insets show the lateral structures of the pulmonary surfactant film throughout the plateau region of the compression isotherms. At each compression stage (monolayer, transition, and multilayer), both the top view and side view of the computer-simulated film and AFM images of the Infasurf film are shown in a column. The lateral dimension of the computer-simulated film is 31 × 31 nm. The scan area of the AFM images is 5 × 3.75 μm;, and the full z-range is 20 nm. Results from the computer simulation and experimental method demonstrate good agreement. Both methods are qualitatively consistent in showing a pressure-driven monolayer-to-multilayer transition during the plateau region of the compression isotherm. Color code used in MD simulations: DPPC in green; POPG in yellow; SP-$B_{1–25}$ in purple; and SP-C in orange.

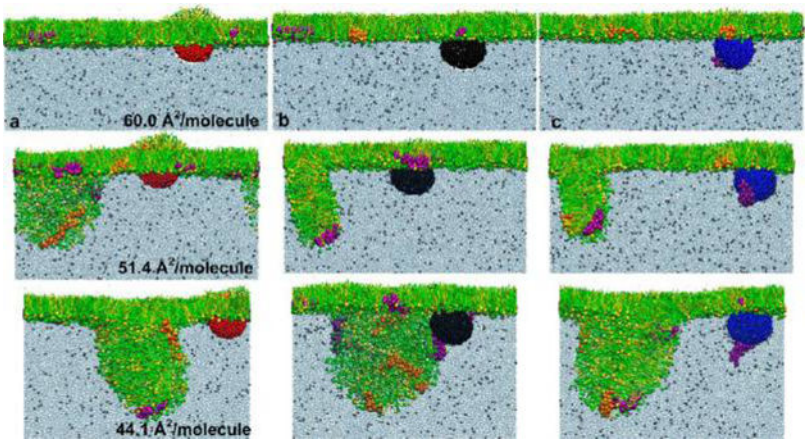

Figure 4.

Computer-simulated interaction between a hydrophilic nanoparticle (NP) of different surface charges and a pulmonary surfactant film under increasing compression. (a–c) The three columns show the interaction between the pulmonary surfactant film and a cationic NP (in red), a neutral NP (in black), and an anionic NP (in blue), respectively. In each column, the pulmonary surfactant film is compressed into three stages (i.e., 60.0, 51.4, and 44.1 $Å^2$/moelcule) that correspond to those shown in Figure 3. It is found that the hydrophilic NP generally penetrates the pulmonary surfactant film regardless of its surface charges. SP-B1–25 (in purple) selectively adsorbs to the surface of the anionic NP and is pulled out of the surfactant film. Color code used in MD simulations: DPPC in green; POPG in yellow; SP-B1–25 in purple; SP-C in orange; cationic particle in red; neutral particle in black; and anionic particle in blue.

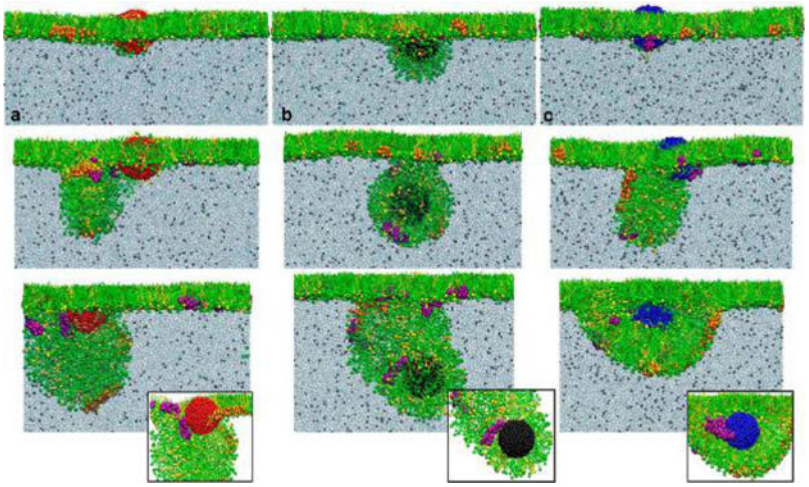

Figure 5.

Computer-simulated interaction between a hydrophobic nanoparticle (NP) of different surface charges and a pulmonary surfactant film under increasing compression. (a–c) The three columns show the interaction between the pulmonary surfactant film and a cationic NP (in red), a neutral NP (in black), and an anionic NP (in blue), respectively. In each column, the pulmonary surfactant film is compressed into three stages (i.e., 60.0, 51.4, and 44.1 $Å^2$/moelcule) that correspond to those shown in Figure 3. It is found that the hydrophobic NP is generally trapped by the pulmonary surfactant film, preferably located at the hydrophobic core of the lipid fold under compression. To clearly demonstrate molecular binding at the NP surface, insets in the last row show interactions between the NP and surfactant proteins/lipids, with the lipid molecules removed from the front view. It clearly shows that only the anionic NP (in blue) can selectively adsorb SP-B1–25 (in purple). For cationic or neutral NPs, although a point contact is possible, $SP\text{-}B_{1–25}$ remains associated with the phospholipids without adsorbing onto the NP surfaces. Color code used in MD simulations: DPPC in green; POPG in yellow; SP-B1–25 in purple; SP-C in orange; cationic particle in red; neutral particle in black; and anionic particle in blue.